CHEMISTRY

Exploiting the Marcus inverted region for first-row transition metal–based photoredox catalysis

Amy Y. Chan[1]†, Atanu Ghosh[2]†, Jonathan T. Yarranton[2], Jack Twilton[1], Jian Jin[1,3], Daniela M. Arias-Rotondo[1], Holt A. Sakai[1], James K. McCusker[2]*, David W. C. MacMillan[1]*

Second- and third-row transition metal complexes are widely employed in photocatalysis, whereas earth-abundant first-row transition metals have found only limited use because of the prohibitively fast decay of their excited states. We report an unforeseen reactivity mode for productive photocatalysis that uses cobalt polypyridyl complexes as photocatalysts by exploiting Marcus inverted region behavior that couples increases in excited-state energies with increased excited-state lifetimes. These cobalt (III) complexes can engage in bimolecular reactivity by virtue of their strong redox potentials and sufficiently long excited-state lifetimes, catalyzing oxidative $C(sp^2)$–N coupling of aryl amides with challenging sterically hindered aryl boronic acids. More generally, the results imply that chromophores can be designed to increase excited-state lifetimes while simultaneously increasing excited-state energies, providing a pathway for the use of relatively abundant metals as photoredox catalysts.

Photoredox catalysis has enabled previously elusive transformations to access value-added products through the selective activation of chemical bonds to generate reactive radical intermediates (*1*, *2*). A key component in the generation of these open-shell intermediates is the photocatalyst, typically a second- or third-row transition metal complex, such as a Ru(II) or Ir(III) polypyridyl species, capable of absorbing visible light (*3*, *4*). Upon visible-light excitation, these metal complexes generate a long-lived charge-transfer excited state with lifetimes on the order of microseconds (*5*–*7*). This longevity enables the excited state to engage in single-electron or energy transfer either with a transition metal catalyst or directly with an organic substrate (*8*, *9*).

Unfortunately, ruthenium and iridium are two of the least abundant elements in Earth's crust. Although some engineered organic dyes have achieved comparable efficiency, tuning their redox windows requires the separate synthesis of each independent catalyst scaffold (*10*, *11*). This lack of flexibility has precluded the use of organic dyes as a complete replacement for transition metal–based photocatalysts. By contrast, tuning the redox properties of metal complexes is often as simple as altering the ligands around the metal center. The wealth of commercially available ligands and knowledge of their impact on the electronic structure of the compound provides a synthetically accessible and predictibale manner in which to tune the redox properties of metal complexes. For this reason, there has been considerable interest in exploiting this flexibility toward the development of cost-effective photocatalysts by using more earth-abundant first-row transition metals (*12*, *13*).

Limitations of first-row metal-based photocatalysis

With few exceptions, little progress has been made toward this goal (*14*–*16*). The smaller ligand-field splitting endemic to first-row transition metals lowers the energy of the ligand-field states below that of the charge-transfer state (*17*). Upon visible-light excitation, these chromophores undergo rapid (subpicosecond) deactivation out of their charge-transfer manifolds (*18*, *19*). Efforts to lengthen the charge-transfer lifetimes of first-row transition metal chromophores by destabilizing the ligand-field manifold with strong, σ-donating ligands (*20*, *21*) tend to require ligands that are challenging to design and synthesize (*22*, *23*). An attractive complementary approach would be to instead leverage the energy stored in these ligand-field excited states. In addition to the economic and environmental benefits of shifting to first-row metal complexes, elucidating the fundamental photophysics and photochemistry of these ligand-field excited states promises enhanced selectivity, as well as unlocking distinct chemical mechanisms and transformations (Fig. 1).

The problem with this approach is caused by the shorter lifetimes typically encountered for ligand-field excited states and how these lifetimes trend with their free energies. For example, the excited-state lifetime of $[Fe(tren(py)_3)]^{2+}$ [where $tren(py)_3$ is a hexadentate polypyridyl ligand] is 55 ns in room-temperature fluid solution. The redox potential (E_0) associated with this compound's lowest-energy excited state was determined to be in the range of 0.6 to 0.7 V versus saturated calomel electrode (SCE) (*24*). Increasing this potential requires increasing the energy of the ligand-field excited state, which can be achieved by replacing $tren(py)_3$ with 2,2′-bipyridine to yield $[Fe(bpy)_3]^{2+}$ though this substitution nearly doubles the energy of the photoactive excited state, its lifetime is decreased to 1 ns under identical conditions. Further increases in excited-state energy will push the lifetime into the subnanosecond regime, severely undercutting the photocatalysts' capacity to engage in bimolecular chemistry.

Leveraging Marcus theory

The correlation between ligand-field strength and excited-state lifetime can be understood within the framework of Marcus theory (*25*–*27*). Although typically invoked in the context of electron-transfer reactions, Marcus theory is a special case of nonradiative decay theory. Its basic principles can be applied to a much wider range of physical and photophysical phenomena, including excited-state relaxation dynamics (*28*). In the Marcus normal region, the zero-point energy of the ligand-field excited state—which equates to its "driving force" for ground-state recovery (ΔG^0)—is smaller in magnitude than the reorganization energy, λ, associated with converting from that state back to the ground state. This leads to a condition in which an increase in ligand-field strength results in an increase in the rate of excited-state relaxation (i.e., shorter excited-state lifetime) (Fig. 2A, left). Photocatalysts designed for energetically demanding reactions need higher excited-state potentials and, thus, increased ligand-field strength. However, the inverse relationship between driving force and excited-state lifetime means that an increase in ligand-field strength also leads to decreased excited-state lifetimes.

In complexes of Co(III), the first-row congener of Ir(III), the ligand-field strength associated with Co(III) is intrinsically larger than that for Fe(II). The observed lifetimes of compounds such as $Co(acac)_3$ and $[Co(en)_3]^{3+}$ of 2 ps and 450 ps, respectively (*29*–*31*), would therefore appear to validate the expectation of decreased lifetime with increasing ligand-field strength. To date, efforts to develop Co(III)-based photocatalysts have been hindered by the lifetimes being too short to effect bimolecular chemistry, with limited exceptions (*32*–*37*). However, upon closer inspection, we realized that a different situation may pertain for Co(III).

The phenomenology of decreasing excited-state lifetime with increasing driving force—the Marcus normal region—remains valid until the driving force and reorganization energy exactly offset each other. This point, where $|\Delta G^0| = \lambda$, is the barrierless region, where the activation energy for the process in question disappears and the rate of the reaction is dictated solely by the electronic coupling between the two states. Marcus' counterintuitive prediction was that, as the driving force is increased beyond this point, the barrier is reintroduced (Fig. 2A, right) and the rate of the process should start to slow down again. This is the inverted region

---

[1]Merck Center for Catalysis at Princeton University, Princeton, NJ 08544, USA. [2]Department of Chemistry, Michigan State University, East Lansing, MI 48824, USA. [3]State Key Laboratory of Chemical Biology, Shanghai Institute of Organic Chemistry, University of Chinese Academy of Sciences, Chinese Academy of Sciences, 345 Lingling Road, Shanghai 200032, China.
***Corresponding author. Email: dmacmill@princeton.edu (D.W.C.M.); jkm@chemistry.msu.edu (J.K.M.).**
†These authors contributed equally to this work.

(*38*, *39*). A recent steady-state spectroscopic study of a series of Co(III) complexes provided quantitative information concerning ligand field-state energetics (*40*). It was determined that the ligand-field strength associated with $[Co(en)_3]^{3+}$ is nearly 0.6 V larger than that of $Co(acac)_3$, yet the data cited above reveals a 100-fold longer excited-state lifetime. We therefore hypothesized that the photophysics of Co(III) complexes might be occurring in the Marcus inverted region (*38*, *39*).

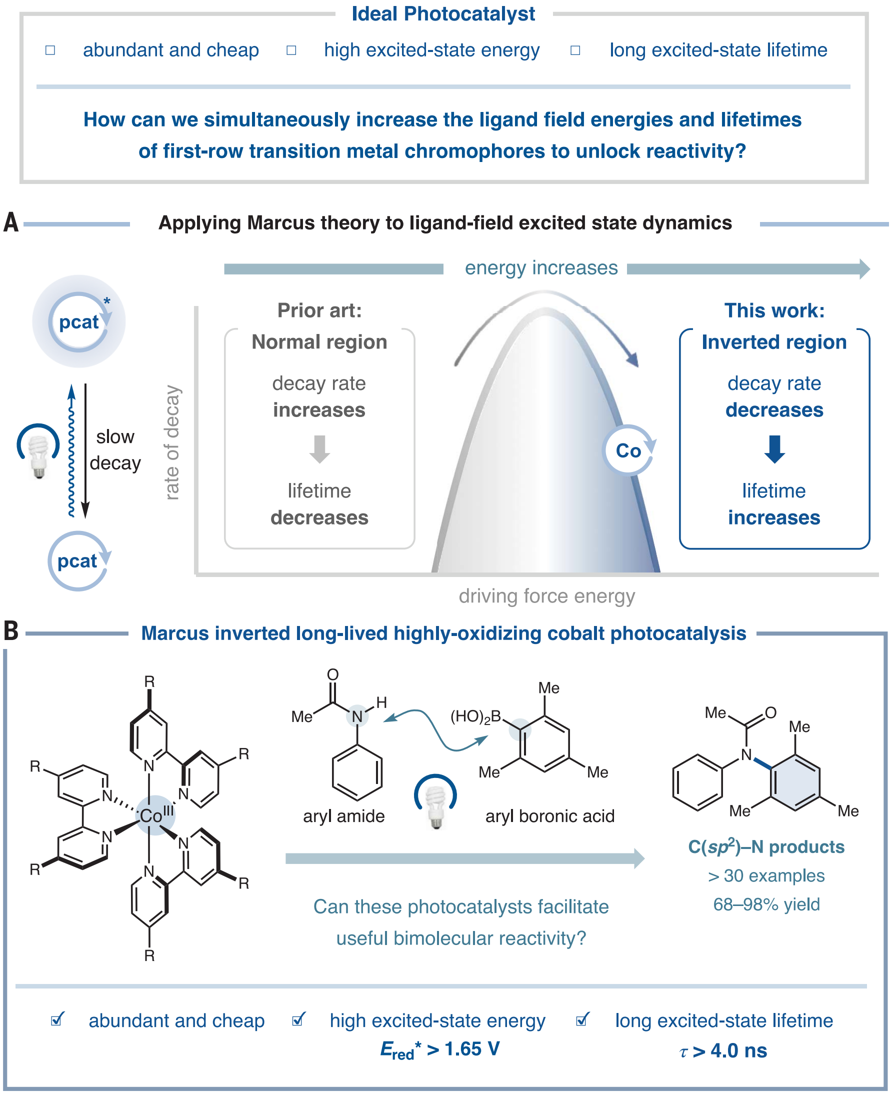

Fig. 1. Exploiting Marcus inverted kinetics for the development of novel Earth-abundant transition metal photocatalysts. (**A**) Marcus inverted dynamics present the opportunity to simultaneously increase excited-state energies and lifetimes. (**B**) Previously unknown class of Marcus inverted cobalt photocatalysts for C(sp^2)–N coupling.

Photophysics of prospective Co catalysts

To examine this possibility, we measured the excited-state lifetime of $[Co(bpy)_3]^{3+}$, a compound characterized by an even stronger ligand field than ethylenediamine, and observed an order-of-magnitude increase in excited-state lifetime to 5.0 ns. We then expanded this effort by using experimentally determined excited-state energies as a guide and measured excited-state lifetimes for a series of homologous Co(III) polypyridyl complexes (*40*). The Marcus plot generated from these measurements is shown in Fig. 2B. The data confirm that the excited-state dynamics of this series of compounds are occurring in the Marcus inverted region, characterized by a reorganization energy of ~4500 cm^{-1} (~0.55 eV), and exhibit lifetimes that should make these complexes viable for bimolecular chemical reactions. Marcus inverted behavior, in which increasing the ligand-field strength builds in more potent excited-state power while simultaneously increasing excited-state lifetimes, opens up enormous possibilities for the use of more Earth-abundant compounds in place of precious metal catalysts for photoredox catalysis.

We first sought to evaluate the competency of these Earth-abundant cobalt complexes as photocatalysts by benchmarking their reactivity to that of precious metal–based photocatalysts. The excited state of the Co(III) ion is expected to be oxidative given that Co(II) is more stable than Co(IV) in simple coordination complexes. In this regard, a transition to Co(III) from Ru(II) or Ir(III) could potentially catalyze similar reactions. We selected reported photoredox transformations that use precious metal photocatalysts to enable the decarboxylative C–H functionalization of heteroarenes, the C–H phosphonylation of arenes, and the α-arylation of ethers (*41*–*43*). We discovered that the performance of our cobalt complexes under unoptimized conditions furnished the desired products in high yields in lieu of iridium or ruthenium polypyridyl complexes as photocatalysts (fig. S15). Furthermore, these cobalt photocatalysts are competent in metallaphotoredox platforms, as demonstrated by replacing iridium with our cobalt complexes in the *N*-alkylation platform achieved through the merger of photoredox catalysis and copper-mediated C–N bond formation (fig. S15) (*44*). Cobalt thus serves as an Earth-abundant replacement for expensive precious metals in metallaphotoredox catalysis. More importantly, we sought to examine if the oxidizing long-lived ligand-field excited state of these cobalt catalysts could unlock reactivity that is elusive with their precious metal counterparts.

Reaction development

C(sp^2)–N bonds are ubiquitous in pharmaceuticals and bioactive molecules, and robust methods to forge such connections are of high interest to synthetic chemists (*45*, *46*). Current methods to achieve these bond connections include palladium-catalyzed Buchwald-Hartwig amination, copper-catalyzed Ullmann-Goldberg coupling, and copper-catalyzed Chan-Evans-Lam coupling (*47*–*49*). These methods have rapidly achieved widespread adoption in industry. The utility of these synthetic transformations stems from the prevalence of nitrogen nucleophiles as readily available building blocks.

However, these methods can be limited owing to the necessity of forcing reaction conditions such as high temperatures, strong bases, and oxidants, resulting in diminished functional group compatibility and poor regioselectivity. Furthermore, the scope of these reactions is restricted to sterically less-hindered coupling partners because of metal-mediated bond breaking and forming processes, including challenging oxidative addition and transmetalation elementary steps. For example, the key elementary step in Chan-Evans-Lam coupling is identified as transmetalation, which goes through a four-membered transition state akin to a σ-bond metathesis (*50*–*52*). In the case of sterically hindered boronic acids, transmetalation is disfavored because of the steric encumbrance

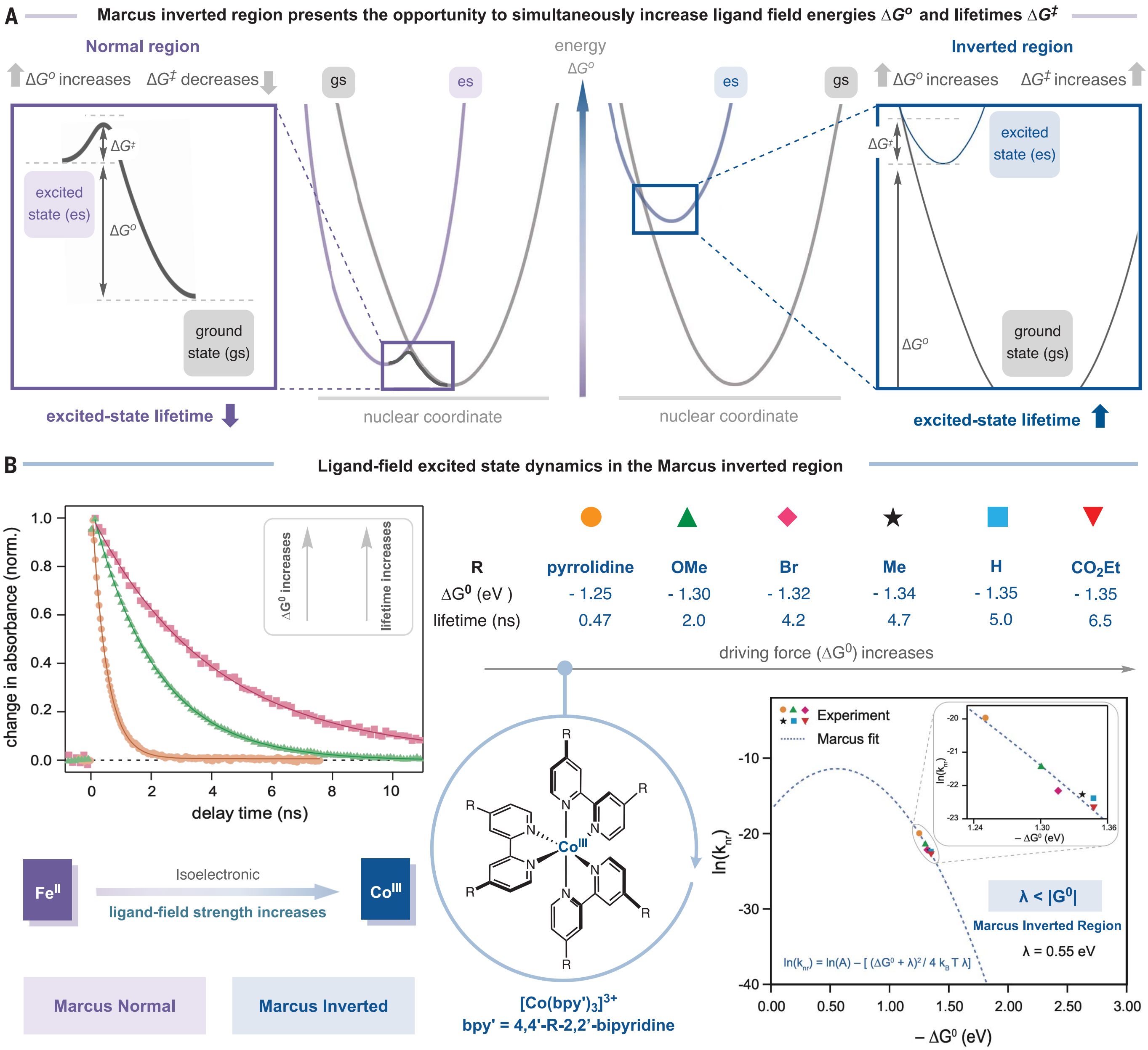

R	● pyrrolidine	▲ OMe	◆ Br	★ Me	■ H	▼ CO_2Et
ΔG^0 (eV)	- 1.25	- 1.30	- 1.32	- 1.34	- 1.35	- 1.35
lifetime (ns)	0.47	2.0	4.2	4.7	5.0	6.5

Fig. 2. Excited-state dynamics of cobalt photocatalysts in the Marcus inverted region. (**A**) Excited-state decay of transition metal complexes as described by Marcus theory. (Left) Marcus normal region where the excited-state lifetime decreases with increasing driving force. (Right) Marcus inverted region where excited-state decay rates slow down and lifetimes increase when the driving force exceeds the reorganization energy associated with ground-state recovery. (**B**) (Left) The excited-state lifetimes of the Co(III) polypyridine complexes systematically increase with increasing driving force for ground-state recovery, which is consistent with Marcus inverted region behavior. (Right) A plot of the experimentally determined excited-state lifetimes as a function of the driving force for ground-state recovery. The latter were obtained from density functional theory (DFT) calculations of the excited-state energies that follow the general trend obtained from experimentally determined spectroscopic transitions. The data are well described by Marcus theory, revealing a reorganization energy for this isostructural series of chromophores of 0.55 eV (4500 cm^{-1}), significantly smaller than the driving force and confirming that the dynamics of this class of compounds occur in the inverted region.

present in the metallocyclobutane transition state. Thus, Chan-Evans-Lam couplings of *ortho*-substituted boronic acid substrates lead to diminished efficiency. Therefore, the challenges of current $C(sp^2)$–N bond forming methods underscore the need to develop distinct methods and mechanistic paradigms for the efficient synthesis of a diverse range of $C(sp^2)$–N bonds of various substitution patterns, especially for sterically demanding cross-coupling partners.

We envisioned that achieving the oxidative coupling of boronic acids with nitrogen nucleophiles such as aryl amides would be extremely desirable given the ready availability of these coupling partners and their compatibility with the highly oxidizing Co(III) photocatalyst (*53*, *54*). Direct oxidation of the nitrogen nucleophile by our Co(III) photocatalysts could furnish an *N*-centered radical, poised to undergo a metal-free *ipso*-substitution with the boronic acid partner to furnish the desired $C(sp^2)$–N product (*55*). The metal-free bond formation would allow for the incorporation of more

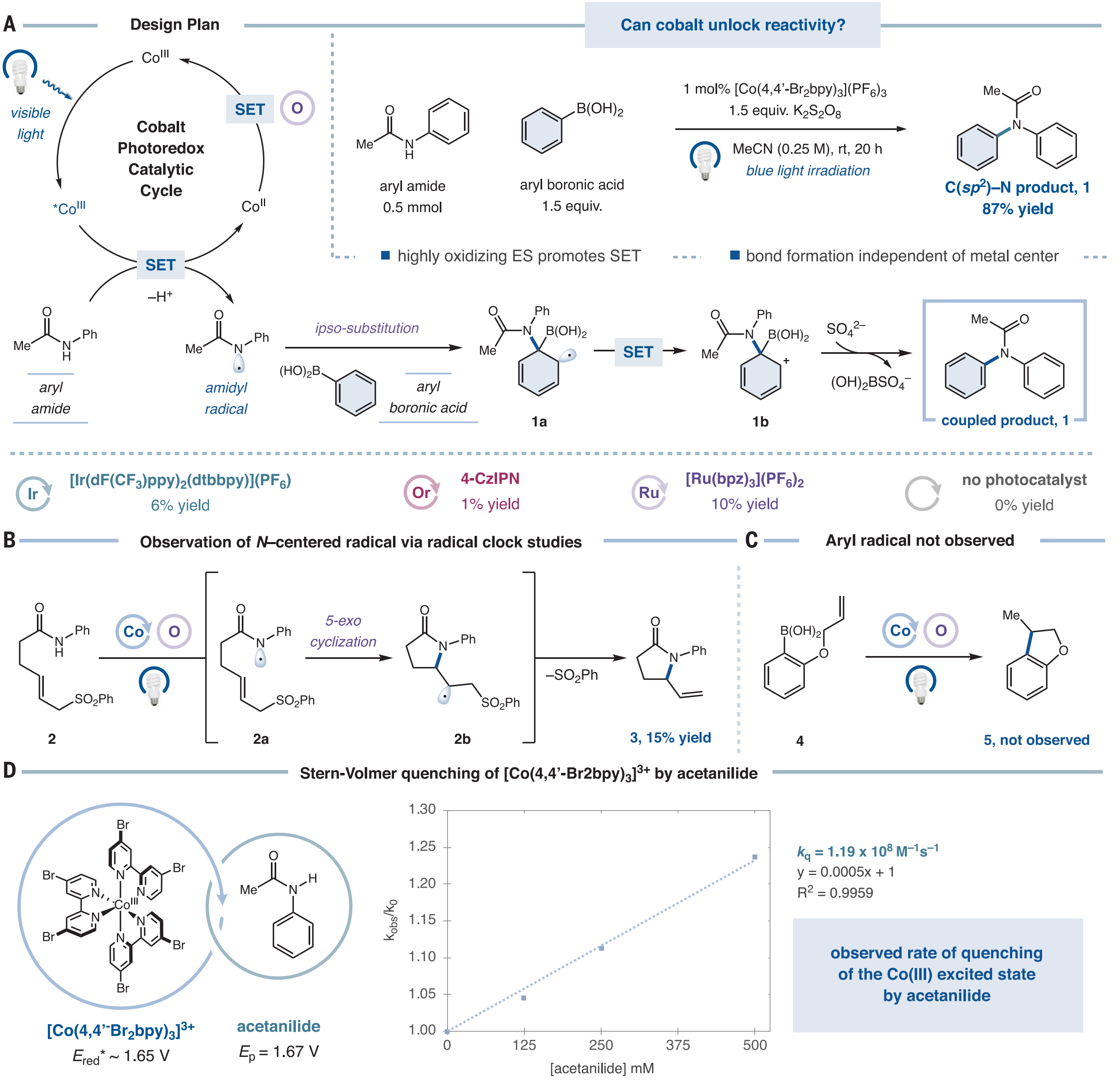

Fig. 3. Application of cobalt photocatalysts toward C–N coupling. (**A**) Proposed catalytic cycle of cobalt photocatalyzed C(sp^2)–N coupling of aryl amide and aryl boronic acids. (**B**) Evidence of the intermediacy of an *N*-centered amidyl radical species. (**C**) Probing the intermediacy of an aryl radical species. (**D**) Stern-Volmer plot of bimolecular quenching kinetics between $[Co(4,4'-Br_2bpy)_3](PF_6)_3$ and acetanilide as determined with time-resolved absorption spectroscopy. The data represents the average of two replicate measuremnts and were fit to a simple linear regression.

sterically encumbered partners. A proposed mechanism for the described reaction is shown in Fig. 3A (left). Photoexcitation generates a highly oxidizing excited-state *Co(III), capable of converting the amide partner to the corresponding amidyl radical. An external oxidant oxidizes the photostable Co(II) complex to Co(III) species, turning over the cobalt catalyst and closing the catalytic cycle. The key C–N bond-formation step proceeds by substitution of the amidyl radical at the *ipso*-carbon of the boronic acid, followed by oxidation of **1a** by Co(III) or the external oxidant and rearomatization of **1b** to furnish the desired product, **1** (*56*).

We explored this idea in the context of the model arylation of amides, notorious for their high oxidation potentials, and were delighted to find that $[Co(4,4'-Br_2bpy)_3](PF_6)_3$ catalyzes the reaction between *N*-phenylacetamide [$E_p = +1.67$ V versus SCE in MeCN (fig. S16)] and phenyl boronic acid in 87% yield (Fig. 3A, right). In fact, the transformation could not be achieved in high yields with well-established Ir(III), Ru(II), or organic photocatalysts (Fig. 3A, bottom), demonstrating the potential of these Co(III) catalysts to unlock distinct reactivity and mechanistic paradigms.

Mechanistic investigation

The ground-state electronic absorption spectrum of $[Co(4,4'-Br_2bpy)_3]^{3+}$ shows a ligand-field transition ($^1A_1 \rightarrow {}^1T_1$) in the visible region

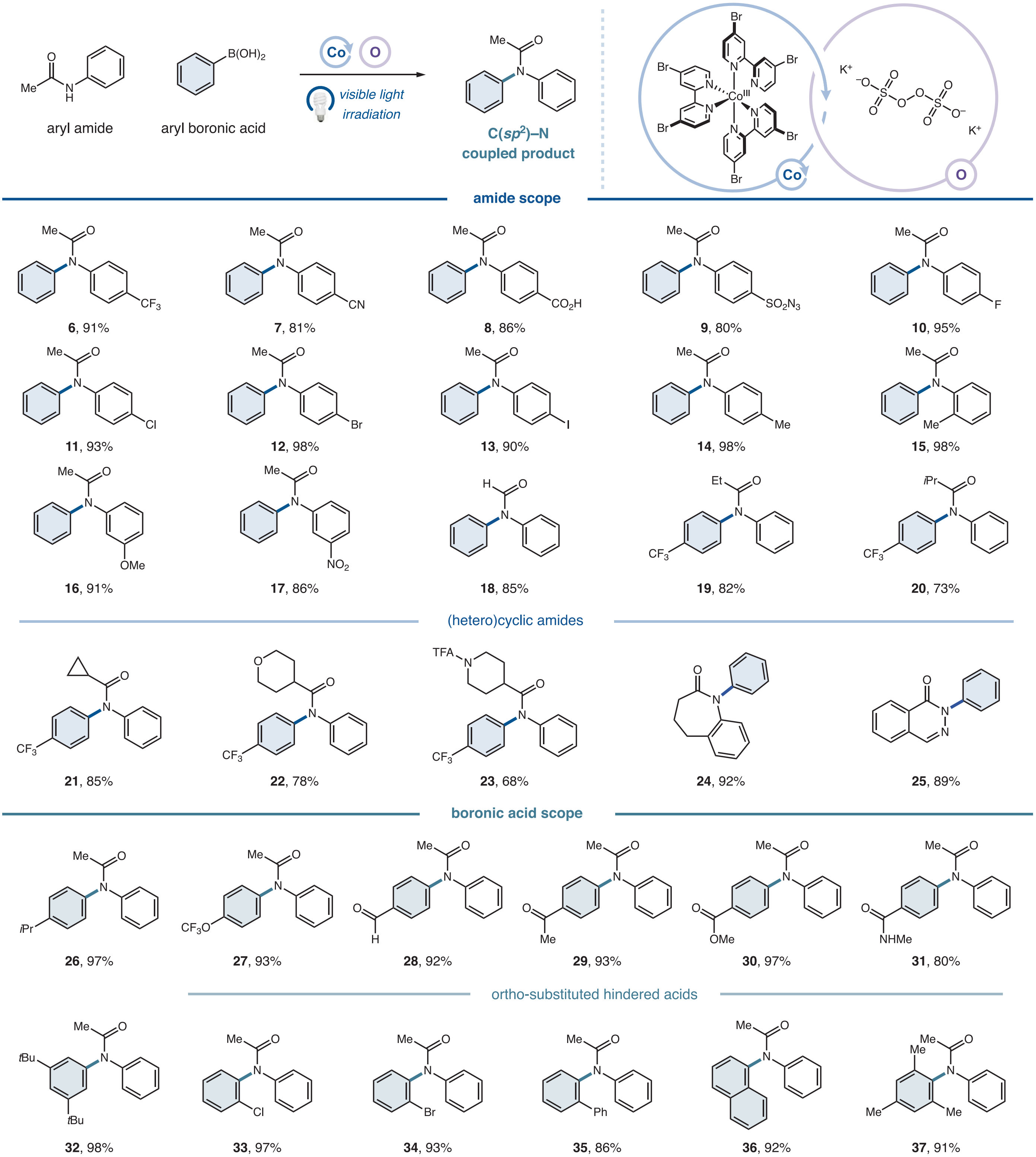

Fig. 4. Scope of cobalt photocatalyzed C(sp^2)–N cross-coupling of aryl amides and aryl boronic acids. All yields are isolated (detailed reaction conditions provided in supplementary materials).

at 461 nm (fig. S6 and table S2). This confirms that the Co(III) complex absorbs visible light to access a ${}^1T_1$ ligand-field excited state, followed by intersystem crossing (ISC) to its lowest-energy ligand-field excited state, which serves as the photoactive species. We carried out a series of measurements following the approach of Meyer and co-workers (*57*), which are designed to bracket the excited-state oxidation potential of [Co(4,4′-Br$_2$bpy)$_3$](PF$_6$)$_3$, which was determined to be E_0 *[Co(III)/Co(II)] ~ +1.65 V versus SCE in MeCN. This cobalt complex is more oxidizing than the highly oxidizing iridium photocatalyst [Ir(dF(CF$_3$)-ppy)$_2$(dtbbpy)](PF$_6$) (E_0 *[Ir(III)/Ir(II)] = +1.21 V versus SCE in MeCN) (*58*).

Upon optimization, we were able to simplify the procedure by complexing and oxidizing the commercially available Co(acac)$_2$ and 4,4′-Br$_2$bpy ligand in situ to form the active catalyst before irradiation (table S3). A variety of oxidants (table S4) could affect the desired chemistry, and persulfate was found to provide the highest yields. Control experiments revealed the necessity of the cobalt salt, bipyridine ligand, and oxidant in the desired transformation; C–N bond formation could not be achieved thermally (table S6). Overall, these findings are consistent with a cobalt-photocatalyzed reaction proceeding by means of a radical pathway.

When amide substrate **2** (E_p = +1.70 V versus SCE in MeCN; fig. S17) (E_p, peak potential) was subjected to the standard reaction conditions, cyclized product **3** was observed in 15% yield, and C(sp^2)–N coupling product was observed in 5% yield (Fig. 3B and fig. S18). In the absence of the boronic acid coupling partner, cyclized product **3** is produced exclusively in 15% yield. Formation of **3** is proposed to proceed through 5-exo cyclization of the amidyl radical **2a** followed by C–S bond homolysis of **2b** to regenerate the double bond (*59*, *60*). No reaction was observed in the absence of cobalt (table S8), supporting its role in the oxidation of the amide and generation of the *N*-centered amidyl radical intermediate. Furthermore, Stern-Volmer bimolecular quenching studies performed with time-resolved absorption spectroscopy indicate that the amide partner quenches the excited state of the Co(III) photocatalyst (Fig. 3D and table S9). The observation of photostable reduced Co(II) photocatalyst in the reaction in situ by means of paramagnetic photo-nuclear magnetic resonance (photo-NMR) confirms the reduction of highly oxidizing Co(III) photocatalyst (fig. S20). Upon subjecting an analogous boronic acid with a pendant olefin **4** to the reaction condition, no cyclized product **5** was observed (*61*–*63*), and only the C(sp^2)–N coupled product was observed in 18% yield (Fig. 3C and fig. S19). These results suggest that amidyl radical formation is an operative and productive pathway, whereas oxidative aryl radical generation is unlikely.

Substrate scope exploration

Lastly, we examined the generality of our discovered protocol. Elucidation of the scope of this transformation demonstrated that a range of steric and electronic substitutions on the aryl coupling partners are compatible in this reaction (Fig. 4). Electron-deficient *N*-aryl amides bearing trifluoromethyl, cyano, carboxy, and sulfonazido groups performed admirably (**6** to **9**, 80 to 91% yield). Moreover, substrates bearing halogen atoms, which can engage in subsequent coupling platforms, reacted to generate the diaryl amide product cleanly under the optimized conditions (**10** to **13**, 90 to 98% yield). Electron-rich acetanilides with functionality at the *ortho*- and *para*- positions also performed well and did not suffer overoxidation (**14** and **15**, 98% yield). Furthermore, placement of an electron-donating or -withdrawing group at the *meta*-position did not reduce efficiency (**16** and **17**, 91 and 86% yields, respectively).

The aryl amide scope can be extended to cyclic and acyclic amides with varying substitution patterns. Formanilide and simple alkyl substituted amides all delivered the desired coupled products in excellent yield (**18** to **20**, 73 to 85% yield). Notably, substrates containing saturated (hetero)cyclic fragments, motifs ubiquitous in medicinal agents, furnished the products in good yields (**21** to **23**, 68 to 85% yield). In addition, benzocaprolactam and phthalazine-1-one served as competent coupling partners (**24** and **25**, 92 and 89% yield, respectively), with the latter suggesting opportunities for selective coupling of other oxidizable nitrogen nucleophiles.

A diverse array of electron-rich aryl boronic acids performed well in this transformation (**26** and **27**, 97 and 93% yield, respectively). Notably, the efficient formation of aldehyde-containing **28** (92% yield) highlights the functional-group compatibility of the transformation because aldehydes can easily be overoxidized to the corresponding carboxylic acids in the presence of metal and potassium persulfate. Boronic acids bearing electron-deficient functionalities, which are challenging in traditional Chan-Evans-Lam couplings, such as ketone and ester groups, also performed well in the reaction (**29** and **30**, 93 and 97% yield, respectively). Also of note is that an *N*-alkyl amide was untouched by the reaction (**31**, 80% yield), presumably because of the higher oxidation potential of *N*-alkyl amides compared with that of *N*-aryl amides. As such, the reaction occurred with high chemoselectivity at the *N*-aryl amide. In addition to *para*-substituted boronic acids, aryl nucleophiles with *meta*-substitutions can be coupled under the optimal conditions (**32**, 98% yield).

Most notably, this method is efficient in coupling sterically encumbered aryl boronic acids. A general issue of Chan-Evans-Lam reactions is *ortho*-substitutions on the aryl organoboron partner, in which increasing steric bulk around the borylated position renders the reaction less effective and often unsuccessful (*64*, *65*). In our developed method, boronic acids bearing chloro, bromo, and phenyl substituents at the *ortho*-position were well accommodated (**33** to **35**, 86 to 97% yields). Extended π-systems, such as naphthyl groups, were also successfully amidated (**36**, 92% yield). The observed high chemoselectivity bodes well for the application of this chemistry in linchpin strategies for the differential functionalization of arene cores. Furthermore, expected steric limitations of Chan-Evans-Lam couplings include 2,6-dimethylphenylboronic acid, which can render the reaction completely ineffective (*66*). However, this di-*ortho* aryl boronic acid was successfully employed in our coupling (**37**, 91% yield). The high tolerance of our transformation toward sterically hindered coupling partners (e.g., *ortho*-substituted aryl boronic acids) supports the proposal that the bond-forming step is not metal-mediated.

Outlook

By increasing both the ligand-field energy and electronics, ground-state recovery of cobalt(III) in the Marcus inverted region can be leveraged as a design principal for other first-row metal-based photocatalysts. This would open up enormous possibilities for the use of Earth-abundant compounds for photoredox catalysis, helping to provide a sustainable future by unlocking previously unknown mechanisms and transformations.

REFERENCES AND NOTES

1. D. A. Nicewicz, D. W. C. MacMillan, *Science* **322**, 77–80 (2008).
2. M. A. Ischay, M. E. Anzovino, J. Du, T. P. Yoon, *J. Am. Chem. Soc.* **130**, 12886–12887 (2008).
3. C. K. Prier, D. A. Rankic, D. W. C. MacMillan, *Chem. Rev.* **113**, 5322–5363 (2013).
4. D. M. Arias-Rotondo, J. K. McCusker, *Chem. Soc. Rev.* **45**, 5803–5820 (2016).
5. M. H. Shaw, J. Twilton, D. W. C. MacMillan, *J. Org. Chem.* **81**, 6898–6926 (2016).
6. S. Campagna, F. Puntoriero, F. Nastasi, G. Bergamini, V. Balzani, *Photochemistry and Photophysics of Coordination Compounds I* (Springer, 2007).
7. L. Flamigni, A. Barbieri, C. Sabatini, B. Ventura, F. Barigelletti, *Top. Curr. Chem.* **281**, 143–203 (2007).
8. J. Twilton *et al.*, *Nat. Rev. Chem.* **1**, 0052 (2017).
9. A. Y. Chan *et al.*, *Chem. Rev.* **122**, 1485–1542 (2022).
10. A. Joshi-Pangu *et al.*, *J. Org. Chem.* **81**, 7244–7249 (2016).
11. N. A. Romero, D. A. Nicewicz, *Chem. Rev.* **116**, 10075–10166 (2016).
12. O. S. Wenger, *J. Am. Chem. Soc.* **140**, 13522–13533 (2018).
13. C. B. Larsen, O. S. Wenger, *Chemistry* **24**, 2039–2058 (2018).
14. M. Pirtsch, S. Paria, T. Matsuno, H. Isobe, O. Reiser, *Chemistry* **18**, 7336–7340 (2012).
15. A. C. Hernandez-Perez, S. K. Collins, *Acc. Chem. Res.* **49**, 1557–1565 (2016).
16. C. E. McCusker, F. N. Castellano, *Inorg. Chem.* **52**, 8114–8120 (2013).
17. J. K. McCusker, *Science* **363**, 484–488 (2019).
18. J. E. Monat, J. K. McCusker, *J. Am. Chem. Soc.* **122**, 4092–4097 (2000).
19. W. Zhang *et al.*, *Nature* **509**, 345–348 (2014).
20. Y. Liu *et al.*, *Chem. Commun.* **49**, 6412 (2013).
21. J. D. Braun *et al.*, *Nat. Chem.* **11**, 1144–1150 (2019).
22. N. Sinha, O. S. Wenger, *J. Am. Chem. Soc.* **145**, 4903–4920 (2023).
23. S. Kaufhold *et al.*, *J. Am. Chem. Soc.* **143**, 1307–1312 (2021).
24. M. D. Woodhouse, J. K. McCusker, *J. Am. Chem. Soc.* **142**, 16229–16233 (2020).
25. R. A. Marcus, *J. Chem. Phys.* **24**, 966–978 (1956).
26. R. A. Marcus, *J. Phys. Chem.* **72**, 891–899 (1968).
27. R. A. Marcus, N. Sutin, *Biochim. Biophys. Acta Rev. Bioenerg.* **811**, 265–322 (1985).
28. P. F. Barbara, T. J. Meyer, M. A. Ratner, *J. Phys. Chem.* **100**, 13148–13168 (1996).
29. L. Ferrari *et al.*, *Front Chem.* **7**, 348 (2019).
30. J. K. McCusker, K. N. Walda, D. Magde, D. N. Hendrickson, *Inorg. Chem.* **32**, 394–399 (1993).
31. C. H. Langford, A. Y. S. Malkhasian, D. K. Sharma, *J. Am. Chem. Soc.* **106**, 2727–2728 (1984).
32. A. K. Pal, C. Li, G. S. Hanan, E. Zysman-Colman, *Angew. Chem. Int. Ed.* **57**, 8027–8031 (2018).
33. P. Rana *et al.*, *Dalton Trans.* **51**, 2452–2463 (2022).
34. Y. N. Gong *et al.*, *J. Am. Chem. Soc.* **142**, 16723–16731 (2020).
35. P. Zhang *et al.*, *J. Mater. Chem. A Mater. Energy Sustain.* **9**, 26286–26297 (2021).

36. W. Liu *et al*., *Angew. Chem. Int. Ed.* **56**, 9312–9317 (2017).
37. S. Tian *et al*., *Nano Res.* **13**, 2665–2672 (2020).
38. J. R. Miller, L. T. Calcaterra, G. L. Closs, *J. Am. Chem. Soc.* **106**, 3047–3049 (1984).
39. G. L. Closs, J. R. Miller, *Science* **240**, 440–447 (1988).
40. J. T. Yarranton, J. K. McCusker, *J. Am. Chem. Soc.* **144**, 12488–12500 (2022).
41. R. Aleyda Garza-Sanchez, A. Tlahuext-Aca, G. Tavakoli, F. Glorius, *ACS Catal.* **7**, 4057–4061 (2017).
42. R. S. Shaikh, I. Ghosh, B. König, *Chemistry* **23**, 12120–12124 (2017).
43. J. Jin, D. W. C. MacMillan, *Angew. Chem. Int. Ed.* **54**, 1565–1569 (2015).
44. N. W. Dow, A. Cabré, D. W. C. MacMillan, *Chem* **7**, 1827–1842 (2021).
45. S. D. Roughley, A. M. Jordan, *J. Med. Chem.* **54**, 3451–3479 (2011).
46. N. A. McGrath, M. Brichacek, J. T. Njardarson, *J. Chem. Educ.* **87**, 1348–1349 (2010).
47. P. Ruiz-Castillo, S. L. Buchwald, *Chem. Rev.* **116**, 12564–12649 (2016).
48. J. X. Qiao, P. Y. S. Lam, *Synthesis* **6**, 829–856 (2011).
49. K. Sanjeeva Rao, T. S. Wu, *Tetrahedron* **68**, 7735–7754 (2012).
50. A. E. King, T. C. Brunold, S. S. Stahl, *J. Am. Chem. Soc.* **131**, 5044–5045 (2009).
51. A. E. King, B. L. Ryland, T. C. Brunold, S. S. Stahl, *Organometallics* **31**, 7948–7957 (2012).
52. J. C. Vantourout, H. N. Miras, A. Isidro-Llobet, S. Sproules, A. J. B. Watson, *J. Am. Chem. Soc.* **139**, 4769–4779 (2017).
53. V. R. Pattabiraman, J. W. Bode, *Nature* **480**, 471–479 (2011).
54. D. C. Blakemore, P. M. Doyle, Y. M. Fobian, *Synthetic Methods in Drug Discovery* (The Royal Society of Chemistry, 2016).
55. K. Zhang, A. Budinská, A. Passera, D. Katayev, *Org. Lett.* **22**, 2714–2719 (2020).
56. I. B. Seiple *et al*., *J. Am. Chem. Soc.* **132**, 13194–13196 (2010).
57. C. R. Bock *et al*., *J. Am. Chem. Soc.* **101**, 4815–4824 (1979).
58. M. M. Alowakennu, A. Ghosh, J. K. McCusker, *J. Am. Chem. Soc.* **145**, 20786–20791 (2023).
59. M. S. Lowry *et al*., *Chem. Mater.* **17**, 5712–5719 (2005).
60. D. C. Miller, G. J. Choi, H. S. Orbe, R. R. Knowles, *J. Am. Chem. Soc.* **137**, 13492–13495 (2015).
61. J. Davies, T. D. Svejstrup, D. Fernandez Reina, N. S. Sheikh, D. Leonori, *J. Am. Chem. Soc.* **138**, 8092–8095 (2016).
62. A. Dickschat, A. Studer, *Org. Lett.* **12**, 3972–3974 (2010).
63. J. W. Lockner, D. D. Dixon, R. Risgaard, P. S. Baran, *Org. Lett.* **13**, 5628–5631 (2011).
64. A. Annunziata, C. Galli, M. Marinelli, T. Pau, *Eur. J. Org. Chem.* **2001**, 1323–1329 (2001).
65. M. J. West, J. W. B. Fyfe, J. C. Vantourout, A. J. B. Watson, *Chem. Rev.* **119**, 12491–12523 (2019).
66. J. F. Dropinski *et al*., *Bioorg. Med. Chem. Lett.* **15**, 5035–5038 (2005).
67. C. Moessner, C. Bolm, *Org. Lett.* **7**, 2667–2669 (2005).

ACKNOWLEDGMENTS

We thank B. T. Boyle, N. W. Dow, O. L. Garry, C. A. Gould, B. X. Li, Y. Liang, W. Liu, C. N. Prieto-Küllmer, and C. P. Seath for helpful scientific discussions; D. G. Oblinsky and M. D. Woodhouse for preliminary spectroscopy; K. Conover and I. Pelczer for NMR support; J. Eng for mass spectroscopy support; P. Jeffrey for crystallography support; and R. Lambert for assistance in the preparation of this manuscript. The content is solely the responsibility of the authors and does not necessarily represent the official views of the National Institute of General Medical Sciences (NIGMS) of the NIH. **Funding:** Research reported in this publication was supported by the NIGMS; the NIH (under award R35GM134897); the Princeton Catalysis Initiative; BioLEC, an Energy Frontier Research Center (US Department of Energy, Office of Science, Office of Basic Energy Sciences, under award DE-SC0019370); and gifts from Janssen, Merck, Bristol Myers Squibb, GenMab, Genentech, and Pfizer. The Rigaku Synergy S Diffractometer was purchased with support from the MRI program by the NSF under grant CHE-1919565 for use at the Center for Crystallographic Research, MSU. A.Y.C. thanks Princeton University, E. C. Taylor, and the Taylor family for an Edward C. Taylor Fellowship. **Author contributions:** J.K.M. and D.W.C.M. conceived of the work. All authors designed the experiments. A.Y.C., A.G., J.T.Y., J.T., J.J., D.M.A.-R., and H.A.S. performed and analyzed the experiments. A.Y.C., A.G., J.T.Y., J.K.M., and D.W.C.M. prepared the manuscript. **Competing interests:** D.W.C.M. declares a financial interest with respect to the Integrated Photoreactor. **Data and materials availability:** Data are available in the supplementary materials. The Cambridge Crystallographic Data Centre (CCDC) website contains the supplementary crystallographic data for this paper under identifiers 2158006 for $[Co(Br_2bpy)_3](PF_6)_2$ and 2158018 for $[Co(Br_2bpy)_3](PF_6)_3$. This data can be obtained free of charge at www.ccdc.cam.ac.uk/data_request/cif, or by emailing data_request@ccdc.cam.ac.uk, or by contacting The Cambridge Crystallographic Data Centre, 12 Union Road, Cambridge CB2 1EZ, UK; fax: +44 1223 336033.

SUPPLEMENTARY MATERIALS

science.org/doi/10.1126/science.adj0612
Materials and Methods
Figs. S1 to S20
Tables S1 to S9
NMR Spectral Data
References (*68–83*)

Submitted 5 June 2023; accepted 28 August 2023
10.1126/science.adj0612

Exploiting the Marcus inverted region for first-row transition metal–based photoredox catalysis

Amy Y. Chan, Atanu Ghosh, Jonathan T. Yarranton, Jack Twilton, Jian Jin, Daniela M. Arias-Rotondo, Holt A. Sakai, James K. McCusker, and David W. C. MacMillan

Science **382** (6667), . DOI: 10.1126/science.adj0612

Editor's summary
Ruthenium and iridium complexes are advantageously tunable photoredox catalysts, but the expense of these precious metals is a drawback to their use. Lighter, more abundant metals have been considered unsuitable because of their anticipated rapid relaxation from photoexcited states. Chan *et al*. report that a cobalt complex with conventional bipyridyl ligands manifests a surprisingly long excited state lifetime, which they attribute to Marcus inverted region behavior (see the Perspective by Yaltseva and Wenger). The Earth-abundant metal is effective at photoredox coupling of aryl amides with aryl boronic acids and more generally opens the door to greater sustainability in this catalyst class.
—Jake S. Yeston

Science (ISSN 1095-9203) is published by the American Association for the Advancement of Science. 1200 New York Avenue NW, Washington, DC 20005. The title *Science* is a registered trademark of AAAS.